Evidence for hydrothermal activity in the Andaman Backarc Basin

P. S. Rao, K. A. Kamesh Raju, T. Ramprasad, B. Nagender Nath, B. Ramalingeswara Rao, Ch. M. Rao and R. R. Nair

Geological Oceanography Division, National Institute of Oceanography, Dona Paula, Goa 403 004, India

Multibeam bathymetric, magnetic, gravity and seismic surveys revealed a complex morphotectonic fabric of the Andaman Backarc Basin with a spreading ridge, several seamounts and faults. The ridge trending SW-NE direction is segmented and shows variations in topography, magnetic and gravity anomalies and seismic structure. The spreading ridge comprises of an inactive northeastern segment and an active southwestern segment. Sampling in the rift valley of the active ridge segment and in a crater of a seamount yielded volcanic rocks which contain vent-like features, broken parts of chimney structures and rocks with disseminate and vein-type metal sulphides. These assemblages, together with the presence of pyrite clusters in the form of rods and irregular lumps in the sediments, are interpreted as evidence for hydrothermal activity in the region, related to backarc spreading and associated volcanism.

SEAFLOOR hydrothermal mineralization results from the dynamic interaction of heat and chemicals between the lithosphere and the seawater at plate boundaries and intraplate volcanic centres. Since the discovery of metalliferous muds in the Red Sea[1,2], search for seafloor hydrothermal mineralization was focused at the mid-oceanic ridge systems and several active and relict hydrothermal fields have been located[3]. The recent drilling into an actively forming massive sulphide deposit in the TAG hydrothermal field of Mid-Atlantic Ridge provided information on the processes of metallogenesis[4,5]. Backarc basins are also considered favourable for the formation of hydrothermal minerals, as the spreading process is believed to be similar. Recently, massive sulphides and other hydrothermal minerals have been discovered at some of the backarc spreading centres and oceanic trenches (Okinawa Trough[6], Lau basin[7,8], North Fiji Basin[9,10]).

The tectonic situation conducive for hydrothermal mineralization in backarc basins arises from a combination of spreading, rifting, faulting and shearing. The Andaman Basin is an evolving backarc basin with a spreading ridge and strike slip faults. The recent volcanic eruptions at the Barren Island, which is a part of the Andaman Arc system, further confirms the tectonic activity in the region. This led us to take up geological and geophysical investigations in the Andaman Backarc Basin.

The Andaman Basin extends from Myanmar in the north to Sumatra in the south and Malay Peninsula in the east to the Andaman and Nicobar islands in the west (Figure 1). Deeper parts surrounded by Malay continental margin, Irrawaddy delta and eastern slope of Andaman Nicobar Ridge form Central Andaman Basin (CAB). Important physiographic features in the CAB are Central Andaman Trough, Sewell Seamount and Alcock Seamount[11]. The bathymetry of the basin significantly controls the sediment deposition. Curray *et al.*[12] reported a spreading centre in the Central Andaman Trough. To evaluate detailed morphology and

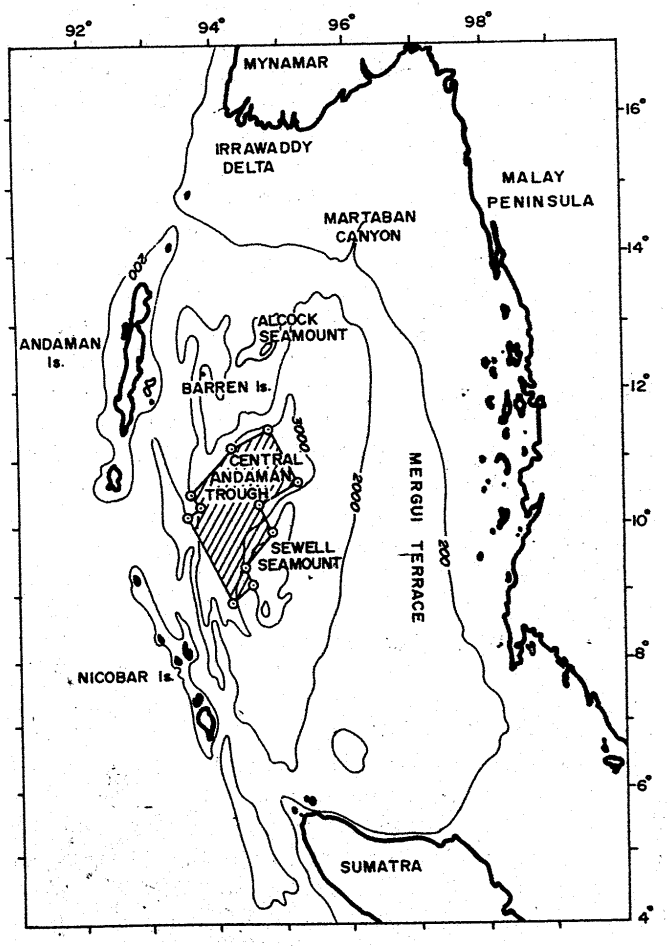

Figure 1. Map showing the study area (hatched) and general physiography of the Andaman Basin.

associated tectonic features of the CAB, we have carried out multibeam bathymetric, magnetic, gravity and seismic surveys covering an area of about 30,000 km^2 between 8°30′N and 11°40′N latitudes and 93°34′E and 95°29′E longitudes. Besides, seabed samples were collected at selected locations to ascertain the presence of hydrothermal activity. Here, we present the initial results of two cruises (SK-89, January 1994; AAS-11, April 1995), which show the evidence for hydrothermal activity in the region.

Bathymetry

The multibeam bathymetric system (Hydrosweep) operates at 15.5 kHz frequency and has a swath coverage equal to twice the water depth[13]. The average depth in the region varied from 2000 to 4100 m. Therefore multibeam swath bathymetric data have been acquired using a track spacing of 3.0 nautical miles in order to achieve near 100% coverage of the survey area. Major morphotectonic features of the Andaman Backarc Basin have been delineated based on the multibeam swath bathymetric data. The area surveyed represents a complex topography, depicting the volcanic arc system and the backarc spreading ridge (Figures 2 *a* and *b*). Several seamounts with heights ranging from 500 to 2000 m are mapped near the volcanic arc region. These seamounts form a chain parallel to the island arc system in the west. The region surveyed is transected by a number of N-S faults (Figure 2 *a*). Prominent among the faults is the West Andaman fault represented by a steep gradient in the bathymetric contours with a down throw of about 2400 m. The other major faults are at 94°E, 94°10′E and 94°25′E longitudes (Figure 2 *a*). The expressions of the Alcock and the Sewell seamounts are noticed in the north and south respectively towards the eastern part of the study area. The bottom topography is smooth in the northeastern portion of the area due to the rapid sediment deposition from the Irrawaddy river. A trench of about 500 m deep is conspicuous in this otherwise flat topographic region. This feature continues toward southwest for about 163 km and corresponds to the Andaman Backarc Spreading Centre (ABSC). This is characterized by a broad 12–15 km isolated rift valley in the northeast and a narrow 8–9 km wide, shallow rift valley in the southwest. The ABSC is segmented at 94°21′E longitude and the segmentation is marked by localized broadening of the rift valley defined by near circular-shaped isobaths. The offset between the northeastern segment (NES) of the rift valley and the southwestern segment (SWS) is about 11.8 km. The rift valley in the NES is well defined with a smooth rift valley floor and along the SWS it is narrow and rugged. The SWS of the spreading centre is associated with off-axis bathymetric highs of about 100 to 200 m.

Gravity and magnetic data

Magnetic and gravity data are acquired along with the multibeam bathymetry. Highly variable magnetic signatures both in terms of the amplitude and frequency are noticed in the study area. Particularly interesting is the magnetic anomaly signature associated with the ABSC (Figure 3). The anomalies along the NES of the spreading centre are remarkably smooth and symmetric seafloor spreading anomalies are absent. Whereas the SWS of the spreading centre has displayed high amplitude anomalies which are analogous to the seafloor spreading type anomalies. Free air gravity in general followed the bottom topography. A consistent low of about 30 mGals is observed along the NES of the spreading centre (Figure 3). The N-S trending faults are well documented

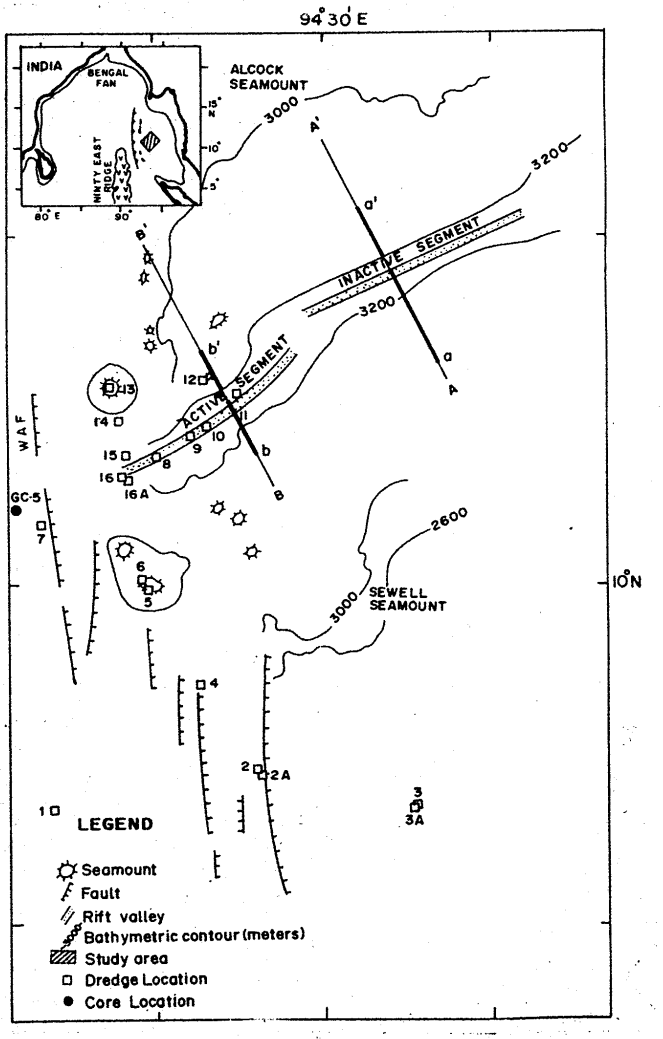

Figure 2 *a*. Major morphotectonic features delineated from multibeam bathymetry, gravity, magnetic and seismic reflection data. WAF denotes the West Andaman Fault. Also shown are the sampling locations and tracks of gravity and magnetic profiles AA′, BB′ and seismic sections aa′, bb′ analysed for this study.

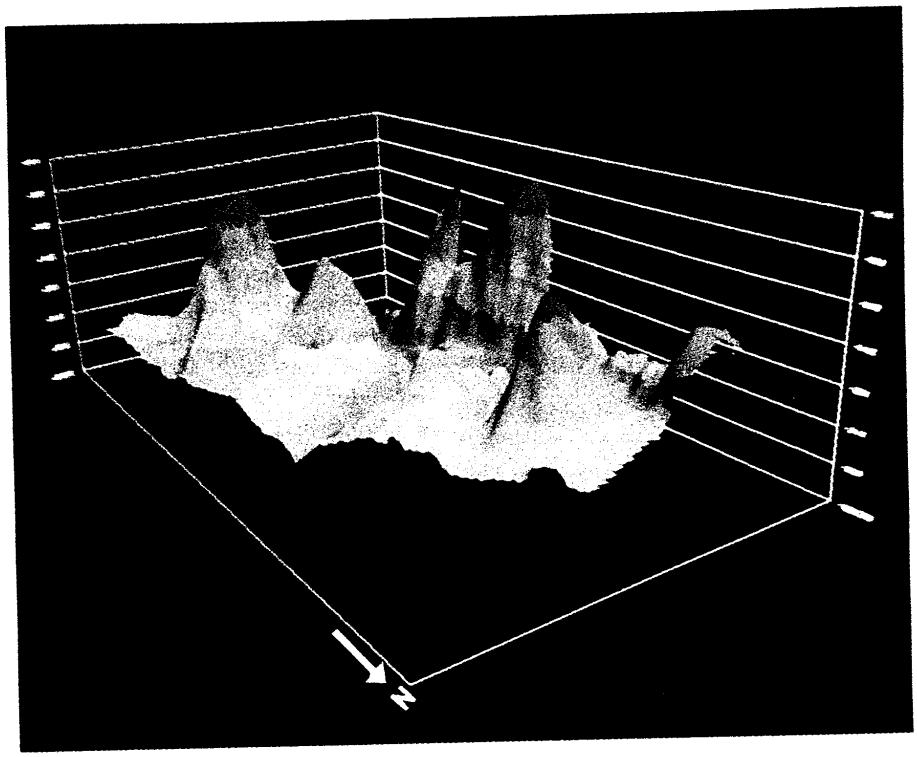

Figure 2 *b*. Sun-illuminated three-dimensional digital terrain model of a part of the area generated from multibeam swath bathymetric data. The seafloor depth is colour coded: dark green is the deepest (4350 m) and red is the shallowest (1525 m). The active segment of the spreading centre is seen as a V-shaped linear trough in the middle with off-axis highs and surrounded by prominent seamounts.

in both magnetic and gravity signatures. Preliminary model studies have enabled identification of seafloor spreading-type anomalies in the SWS of the spreading centre. Anomalies 2, 2A and 3 are distinct along the line BB′ (Figure 3) over the active segment. The oldest identifiable anomaly in this region is 5A, which corresponds to an age of about 11.55 my (ref. 14). The average half spreading rate computed is about 1.86 cm/yr and comparable with the results of Curray *et al.*[12]. The topographic fabric and the magnetic signature associated with the SWS of the rift valley appears to be a manifestation of a probable evolving new rift. These observations indicate that the SWS of the spreading centre is presently active and the NES is inactive.

Seismic data

Single channel air-gun seismic reflection data have been acquired in the study area. The seismic lines were planned across the active and inactive segments of the spreading centre and a seismic line was shot along the axis of the rift valley. The seismic records across the active and inactive segments have shown distinct variations in the sedimentation pattern and thickness (Figure 4). Across the inactive segment, a thick pile of sediments is present over the flanks of the rift valley. The deepest reflector in this region is found to be at about 5.08 s (TWT). The sediment thickness is about 1.23 s (TWT), which translates to about 1.8 km considering an average velocity of 3000 m/s. Near symmetrically spaced upturned sequence of reflectors are seen on either side of the inactive segment (NES) of the rift valley. The rift valley floor is filled with sediments about 0.6 km thick, which are seen as subparallel reflectors extending up to 5.4 s (TWT) on the seismic section (Figure 4).

The seismic section across the rift valley of the active segment (Figure 4) depicts thin or no sediment cover within the rift valley floor. Strong hyperbolic reflectors seen over a short distance within the rift valley over

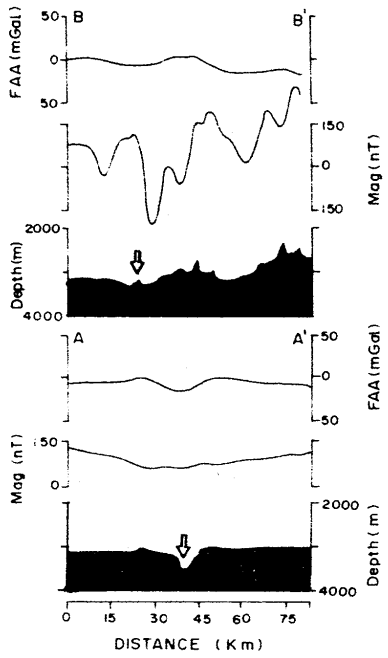

Figure 3. Bathymetric, magnetic and gravity profiles over inactive (AA′) and active (BB′) segments of the spreading centre. Arrow denotes the rift valley.

the intra-valley high probably indicate an evolving crust in the region.

Seabed samples

Sampling stations were selected based on local topography and tectonic features delineated by the integrated analyses of multibeam bathymetry, magnetic, gravity and seismic data. Dredging was carried out at 16 stations along the axis and flanks of the rift valley, on the fault planes and on the seamounts (Figure 2 *a*). Table 1 gives details of sample location, water depth and sample description. The rocks collected from the rift valley are fresh and altered basic igneous rocks and comprise of massive, vesicular and ropy lava types and breccia. Petrographic observations suggest that the rocks are mainly basalts/olivine basalts. However, a dredge haul from a fault plane (station 2A) brought tholeiites (plagioclase and pigeonite augite). Some of these rocks have thin manganese oxide coatings and often exhibit alteration rims. Dredging on a seamount north of the active ridge segment (station 13) yielded large quantity of fresh and altered pumice and no other rock types. Recovery of various types of rocks, ranging from acidic

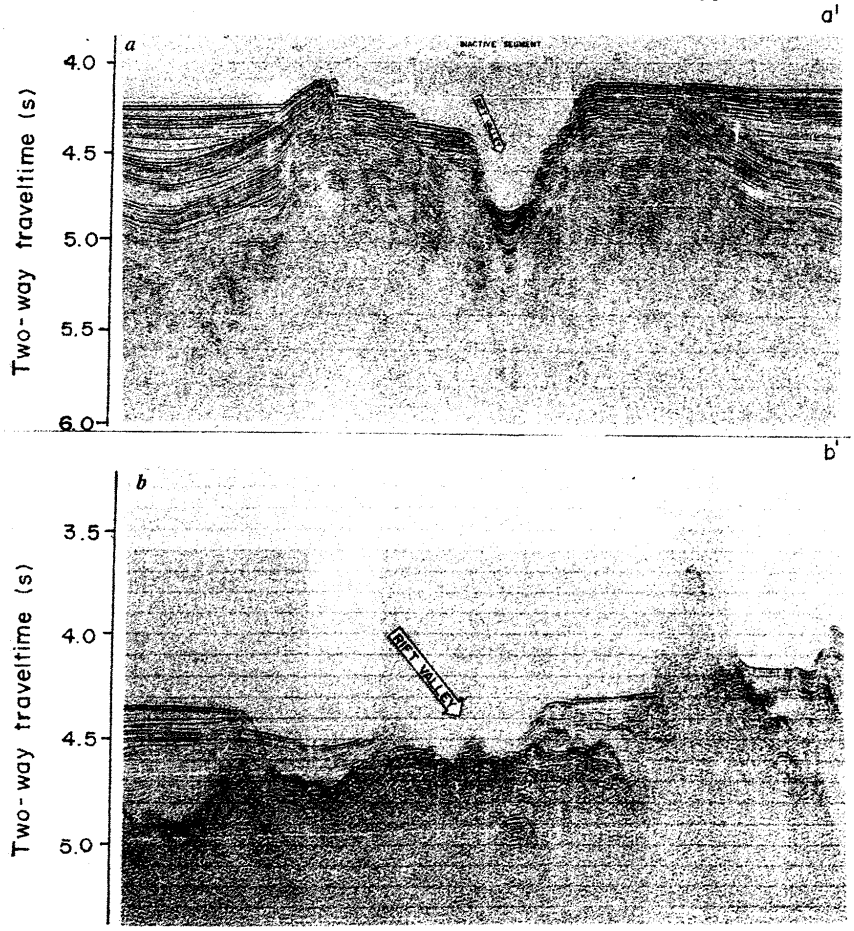

Figure 4. Seismic sections across inactive (aa′) and active (bb′) segments of the spreading centre.

Table 1. Details of dredge samples

Dredge station no.	Geological setting	Water depth (m)	Sample description
1	Fault plane	3137–3219	No recovery
2	Fault plane	2972–2995	No recovery
2A	Fault plane	3031–3152	Weathered and fresh olivine basalts, tholeiites, porphyritic and glassy to cryptocrystalline. Some rocks are coated with Fe–Mn oxides
3	Seamount	792–831	No recovery
3A	Seamount	691–1016	No recovery
4	Fault plane	2951–2968	Sediment
5	Seamount	1628–1631	No recovery
6	Seamount crater	1638–1646	Large chunks of dark and light-coloured rocks, angular to sub-angular and sub-rounded. Part of talus, mostly pyroclastic. Some rocks have disseminated and vein-type metal sulphides
7	Fault plane	1884–2472	Fine grained reddish brown hard clay stones and feldspathic sand stones
8	Rift valley	3677–3765	Fresh, porphyritic olvine basalts with glassy top. Some rocks show zonation rims
9	Rift valley	3353–3386	Massive, vesicular basalts. Fragments of chimney-like feature. Occasionally Fe–Mn oxide precipitates are seen
10	Rift valley axial high	2929–2979	Ropy lava, vesicular basalts, rock with vent-like openings. Some rocks show yellowish tinge
11	Rift valley	3286–3346	Ropy lava, vesicular basalts, rocks with iron oxide coatings
12	Off-axis seamount	2635–2970	Sediment
13	Seamount	1615–1710	Fresh and altered pumice. Some pumice are coated with Fe–Mn oxides
14	Outer flank of rift valley	2510–3148	Pumice and weathered basalts
15	Inner flank of rift valley	3181–3184	Layered and consolidated sediments; Fe–Mn oxide coatings
16	Inner flank of rift valley	3598–3805	No recovery
16A	Inner flank of rift valley	3256–3539	Ropy lava, agglomerate type rocks, vesicular basalts.

(pumice) to basic nature may indicate either different episodes of volcanic activity or the inhomogeneous nature of the melt.

Of particular interest is the presence of fragments of chimney-like structure and a large rock with holes (Figure 5), collected from the axis of the rift valley and a 200 m axial high respectively (stations 9 and 10). The chimney fragments are semicircular with varying lengths and appear to be part of a pipe-like structure. By extrapolating the curvature of the fragments, we deduce that the inner diameter of the pipe was about 8 cm before fragmentation. Morphologically the fragments have a very rough, shiny black fragile outer surface and hard, dull inner surface with zonation. The inner surface has a lining of secondary formations probably formed under different temperature and cooling conditions. Deposition of manganese and iron oxides is noticed occasionally on the inner surface of the pipe fragments. The holes in the rock from the axial high are 3–5 cm in diameter, continuous, interconnected and appear to be conduits for the passage of solutions. The inner wall of the passages is similar to that of the fragments described earlier, and probably formed under similar conditions. Patches of thin layer of sediments are deposited in the passages at certain places. The presence of sediments in the conduits of the rock and manganese and iron oxides on the inner walls of the chimney fragments suggests that these were part of a vent system which was active in the past.

Dredging in the crater of a seamount, south of the

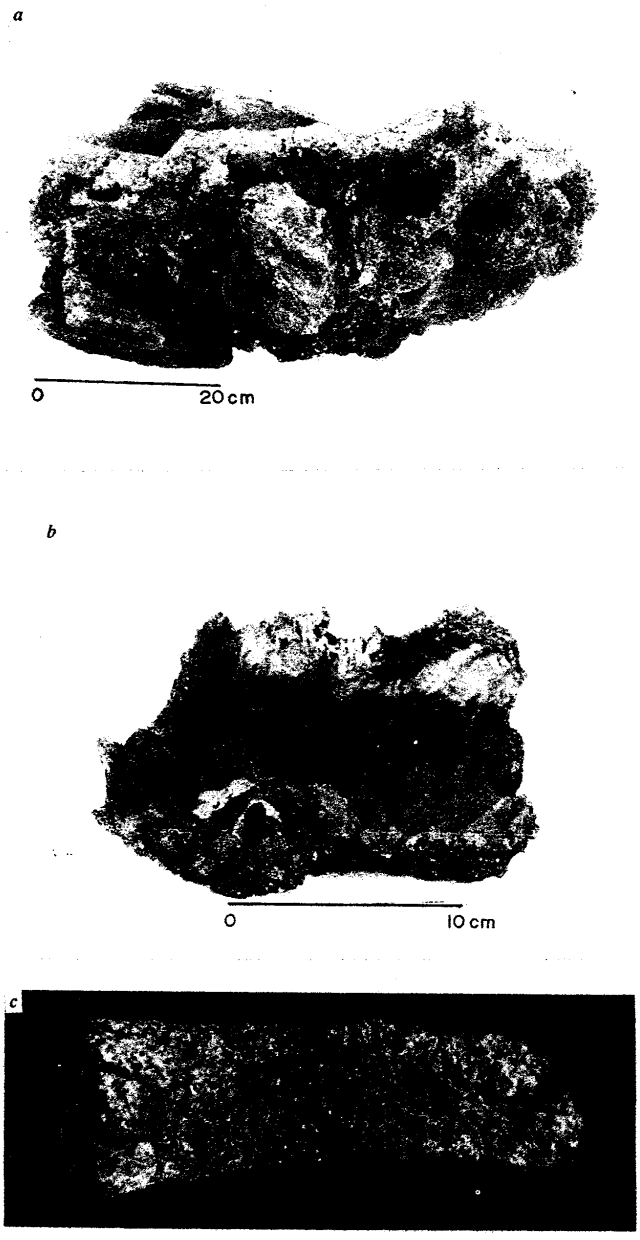

Figure 5. *a*, Volcanic rock dredged from the active ridge segment showing vent-like openings. *b*, Part of a chimney-like feature recovered in a dredge haul from the active ridge segment. *c*, A 3.4-cm long pyrite rod recovered from a sediment core (GC-5) adjacent to the active ridge segment.

rift valley (station 6) yielded light, grey and dark coloured angular and subangular rocks which are part of talus. Microscopically, some of these rocks are very fine grained with 60 to 70% glass, little quartz and calcite phenocrysts. Several rocks from this location contain disseminated and vein-type shiny particles. Microscopic observation of these particles reveals that they are metal sulphides, mostly in the form of pyrite (Figure 6). X-ray back scatter images of the shiny

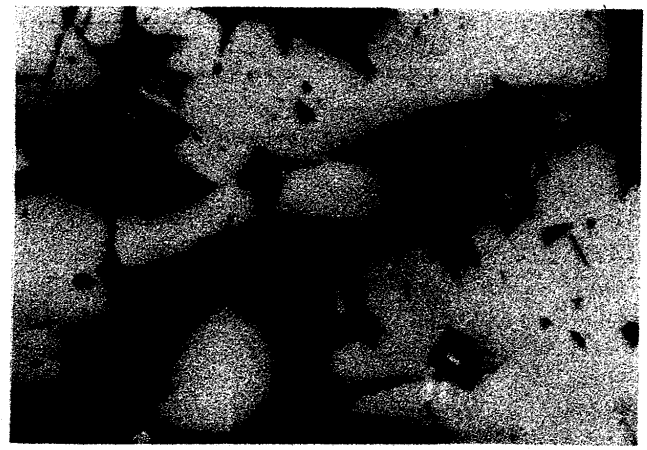

Figure 6. Reflected light photomicrograph showing euhedral pyrite grains (uncrossed × 100).

particles confirm that they are iron sulphides embedded in silicate matrix. The veins appear to be fracture fillings of hydrothermal precipitates.

Heavy metalliferous rods and lumps admeasuring 2–3.5 cm (Figure 5) were recovered in the sediments adjacent to the active segment of the rift valley (station GC-5). X-ray diffraction analysis (CuKα target, 2°2θ/min) revealed that these objects consist of pyrite and no other mineral phase. Further chemical analysis and SEM observations confirm that the metalliferous lumps are devoid of other minerals except pyrite.

Concluding remarks

Based on multibeam bathymetry, gravity, magnetic and seismic data, an 80 km long active spreading centre and several submarine volcanoes and seamounts have been delineated in the Andaman Backarc Basin. Sediment and rock samples in the vicinity of the active spreading centre and a cratered seamount revealed the presence of pyrite lumps, disseminated vein-type pyrite and rocks with vents and chimney fragments. These findings are clear evidences for hydrothermal activity in the region. A detailed multi-disciplinary study, supported by deep-sea photographic survey and close grid sampling is planned to delineate the extent of hydrothermal mineralization in the Andaman Backarc Basin.

1. Miller, A. R., Densmore, C. D., Degens, E. T., Pocklington, R. and Jokela, A., *Geochim. Cosmochim. Acta*, 1966, **30**, 341–359.
2. Degens, E. T. and Ross, D. A. (eds), *Hot Brines and Recent Heavy Metal Deposits in the Red Sea*, Springer-Verlag, New York, 1969, pp. 600.
3. Rona, P. A. and Scott, S. D., *Econ. Geol.*, 1993, **88**, 1935–1975.
4. Humphris, S. E. *et al.*, *Nature*, 1995, **377**, 713–716.
5. Koski, R. A., *Nature*, 1995, **377**, 679–680.
6. Halbach, P., Pracejus, B. and Marten, A., *Econ. Geol.*, 1993, **88**, 2210–2225.

7. von Stackelberg, U., *Mar. Min.*, 1990, **9**, 135–144.
8. Fouquet, Y., von Stackelberg, U., Charlou, J. L., Erzinger, J., Herzig, P. M., Mühe, R. and Wiedicke, M., *Econ. Geol.*, 1993, **88**, 2154–2181.
9. Bendel, V., Fouquet, Y., Auzende, J-M., Lagabrielle, Y., Grimaud, D. and Urabe, T., *Econ. Geol.*, 1993, **88**, 2237–2249.
10. Binns, R. A. and Scott, S. D., *Econ. Geol.*, 1993, **88**, 2226–2236.
11. Rodolfo, K. S., *Geol. Soc. Am. Bull.*, 1969, **80**, 1203–1230.
12. Cumy, J. R., Moore, D. G., Lawver, L. A., Emmel, F. J., Raitt, R. W., Henry, M. and Kieckhefer, R., in *Geological and Geophysical Investigations of Continental Margins*, Am. Assoc. Petrol. Geol. Memoir, 1979, vol. 29, pp. 189–198.
13. Gutberlet, M. and Shenke, H. W., *Mar. Geodesy*, 1989, **33**, 1–23.
14. Berggren, W. A., Kent, D. V., Flynn, J. J. and Van Couvering, J. A., *Geol. Soc. Am. Bull.*, 1985, **96**, 1407–1418.

ACKNOWLEDGEMENTS. We thank Dr S. Dost, Director, NIO, for encouragement and providing funds to charter research vessel AA Sidorenko; Department of Ocean Development, New Delhi for ship time onboard ORV Sagar Kanya; Dr R. Natarajan, NGRI, for X-ray back-scatter analysis; Prof. A. S. R. Swamy, Andhra University, for SEM photos; Prof. V. C. Chavadi, Karnatak University, for thin section observations; Dr A. S. Venkatesh, Indian School of Mines, for one microscopic study and Mr G. Prabhu, NIO for XRD analysis.

Received 12 December 1995; revised accepted 8 February 1996